

Star Formation at Very Low Metallicity. II: On the Insignificance of Metal-Line Cooling During the Early Stages of Gravitational Collapse

A.-K. Jappsen^{1,2}, S. C. O. Glover^{2,3}, R. S. Klessen^{4,2}, M.-M. Mac Low³

ABSTRACT

We study the influence of low levels of metal enrichment on the cooling and collapse of ionized gas in small protogalactic halos using three-dimensional, smoothed particle hydrodynamics simulations. Our initial conditions represent protogalaxies forming within a fossil H II region, a previously ionized H II region which has not yet had time to cool and recombine. Prior to cosmological reionization, such regions should be relatively common, since the characteristic lifetimes of the likely ionizing sources are significantly shorter than a Hubble time. We show that in these regions, H₂ is the dominant and most effective coolant, and that it is the amount of H₂ formed that determines whether or not the gas can collapse and form stars.

At the low metallicities ($Z < 10^{-3} Z_{\odot}$) thought to be associated with the transition from Population III to early Population II star formation, metal-line cooling has an almost negligible effect on the evolution of low-density gas, altering the density and temperature evolution of the gas by less than 1% compared to the metal-free case at densities below 1 cm^{-3} and temperatures above 2000 K. Although there is evidence that metal-line cooling becomes more effective at higher density, we find no significant differences in behaviour from the metal-free case at any density below our sink particle creation threshold at $n = 500 \text{ cm}^{-3}$. Increasing the metallicity also increases the importance of metal-line cooling, but it does not significantly affect the dynamical evolution of the low-density gas

¹Canadian Institute for Theoretical Astrophysics,
University of Toronto, Toronto, ON M5S 3H8, Canada; jappsen@cita.utoronto.ca

²Astrophysikalisches Institut Potsdam,
14482 Potsdam, Germany; sglover@aip.de

³Department of Astrophysics, American Museum of Natural History,
New York, NY 10024-5192; mordecai@amnh.org

⁴Zentrum für Astronomie der Universität Heidelberg, Institut für Theoretische Astrophysik,
69120 Heidelberg, Germany; rklessen@ita.uni-heidelberg.de

until $Z \sim 0.1 Z_{\odot}$. This result holds regardless of whether or not an ultraviolet background is present.

Subject headings: galaxies: formation — molecular processes — stars: formation

1. Introduction

Within the framework of cold dark matter (CDM) cosmology the formation of structure proceeds in a hierarchical fashion. At high redshifts, low-mass halos with virial temperatures less than $\sim 10^4$ K are abundant. The cooling of primordial gas in these halos is regulated by molecular hydrogen, as H_2 is the only coolant present in significant quantities that remains effective at temperatures below 10^4 K (Saslaw & Zipoy 1967; Peebles & Dicke 1968; Matsuda et al. 1969). Tegmark et al. (1997) developed analytic methods to model early baryonic collapse via H_2 cooling. Numerical studies of the formation of primordial gas clouds and the first stars indicate that this process likely began as early as $z \sim 30$ (Abel et al. 2002; Bromm et al. 2002). Yoshida et al. (2003) further utilized simulations to develop a semi-analytic model based on the Tegmark et al. (1997) methods and included the effects of dynamical heating caused by the thermalization of kinetic energy of infall into a deepening potential. Both approaches suggest that only gas in halos more massive than some critical mass M_{crit} will cool effectively. Much of this work has recently been reviewed by Bromm & Larson (2004), Ciardi & Ferrara (2005), and Glover (2005).

Population III stars are the first potential producers of UV photons that can contribute to the reionization process and are the first producers of the metals required for the formation of population II stars. An important question is whether small protogalaxies that formed within the relic H II regions left by these first stars could form stars themselves, or whether the elevated temperatures and fractional ionizations found in these regions suppressed star formation until larger protogalaxies formed. In a recent analytical study, Oh & Haiman (2003) argue that the first stars injected sufficient entropy into the early intergalactic medium (IGM) by photoionization heating and supernova explosions to strongly suppress further star formation inside low-mass protogalactic halos in the affected regions. On the other hand, previous numerical work by Ricotti et al. (2002) and O’Shea et al. (2005), as well as our own simulations of hot, ionized gas in small protogalactic halos, show that gravitational collapse mediated by H_2 cooling remains possible in such regions, within protogalaxies with masses above a certain threshold, implying that in these systems star formation is not strongly suppressed.

A further form of negative feedback that must be taken into account comes from UV

photons within the Lyman-Werner bands of H_2 , which are produced in large numbers by massive population III stars and which can photodissociate H_2 , thereby quenching molecular hydrogen cooling and delaying the cooling and collapse of the primordial gas (Haiman et al. 2000; Machacek et al. 2001; Glover & Brand 2001; Johnson et al. 2007).

Metals produced by the first stars will also be injected into some fraction of the ionized volume, and so will be present in gas falling into new or existing protogalactic halos. The question then arises as to how this low level of metal enrichment affects the ability of the gas to cool and collapse. Bromm et al. (2001) studied the collapse of cold, metal-enriched gas and argued that there exists a critical metallicity Z_{crit} below which the gas fails to undergo continued collapse and fragmentation. However, their simulations did not allow for H_2 formation and H_2 cooling, which is expected to play an important role, unless the external UV background is extremely strong. Also, by starting with cold gas, they implicitly assume that no extra entropy or energy has been added to the gas during its enrichment; although, as Oh & Haiman (2003) have shown, this is unlikely to be the case. We reexamine this question using more appropriate initial conditions and a more detailed treatment of the cooling and chemistry of the metal-poor gas.

We present simulations showing that metals play a dominant role in regulating the cooling of ionized gas in small protogalactic halos only for metallicities $Z \sim 0.1 Z_{\odot}$ or greater. At lower metallicities, the metals have little effect and the question of whether or not gas in a particular halo collapses is entirely determined by the amount of H_2 forming in that halo. We reach the same conclusion regardless of whether or not the gas is illuminated by a Lyman-Werner UV background, as in the absence of H_2 the metals themselves do not provide enough cooling to allow the gas to collapse.

2. Simulations

2.1. Numerical Method

To help us to assess the influence of metals on the cooling and collapse of gas in small protogalactic halos, we performed a number of numerical simulations. During collapse, gas increases in density by several orders of magnitude, and so is best simulated by a numerical method with a high dynamical range. We therefore chose smoothed particle hydrodynamics (SPH). Excellent overviews of the method, its numerical implementation, and some of its applications are given in reviews by Benz (1990) and Monaghan (1992, 2005). We use version 1 of the parallel code GADGET, designed by Springel et al. (2001). SPH is a Lagrangian method for simulating astrophysical flows, in which the fluid is represented by an ensemble of

particles, with flow quantities at a particular point obtained by averaging over an appropriate subset of neighboring SPH particles. As particle time steps in an SPH code are constrained by the Courant condition, they grow increasingly short as more particles cluster in high-density regions. Replacing dense cores with artificial sink particles can therefore lead to a considerable increase in computational performance, allowing the dynamical evolution of the gas to be followed over many free-fall times. In the runs presented here we introduce sink particles according to the prescription of Bate et al. (1995). Sink particles are created once the density rises above 500 cm^{-3} and are endowed with an accretion radius of 5 pc. On every time step, any gas within this accretion radius that is gravitationally bound to the sink particle is accreted by it. The design and implementation of our sink particle algorithm is discussed in more detail in Jappsen et al. (2005).

2.2. Chemistry and Cooling

We have further modified GADGET to allow us to follow the nonequilibrium chemistry of the major coolants in both primordial and low-metallicity gas. Our chemical model is a simplified version of the general model for low-density, low-metallicity gas presented in Paper I (Glover & Jappsen 2007). In our simplified network, we follow the chemistry of twelve separate species: free electrons, H^+ , H^- , H , H_2^+ , H_2 , C , C^+ , O , O^+ , Si , and Si^+ . The more detailed model in Paper I also follows the chemistry of He , He^+ , Si^{++} , D , D^+ , and HD . However, the helium and Si^{++} chemistry are important primarily at temperatures $T \gtrsim 10^4 \text{ K}$, or if the gas is partially ionized by X-rays or cosmic rays, while the deuterium chemistry is only significant at temperatures $T < 200 \text{ K}$, which are only reached in a few of our simulations, and so the neglect of these additional reactions reduces the computational cost imposed by the chemistry without significantly affecting our main results. The other simplification we made here compared to the model of Paper I is the neglect of photochemical reactions involving photons more energetic than 13.6 eV; specifically, we omit the photoionization of H , He , H_2 , O , and Si^+ (reactions 48, 50, 54, 57, and 59 in Paper I). We omit these reactions because we assume that during the simulations, our model protogalaxies are shielded by the neutral hydrogen in the intergalactic medium from any external sources of ionizing radiation. A full list of reactions included in the chemical network used in the simulations presented in this paper is given in Table 1. Further details (including a discussion of why these particular reactions were chosen and full details of the rate coefficients used) are given in Paper I.

In implementing this chemical network within GADGET, we made the decision to follow the nonequilibrium abundances of H_2 , H^+ , C^+ , O^+ , and Si^+ and use conservation laws for charge and element abundance to track H , e^- , C , O , and Si . The remaining two species, the

H^- and H_2^+ ions, have very short chemical equilibrium timescales and hence were assumed, for simplicity, to reach equilibrium instantaneously. To compute the rate of photochemical reactions (such as the photodissociation of H_2) in runs in which an ultraviolet background is present, we assume a background spectrum that has the shape of a 10^5 K black body (as should be typical of the brightest Population III stars; see e.g. Cojazzi et al. 2000), cut off at energies greater than 13.6 eV to account for absorption by neutral hydrogen in the IGM. We quantify the strength of the background by fixing the flux at the Lyman limit: $J(\nu_\alpha) = 10^{-21} J_{21} \text{ erg s}^{-1} \text{ cm}^{-2} \text{ Hz}^{-1} \text{ sr}^{-1}$. A list of the resulting photochemical rates is given in Table 2, computed using the cross sections listed in Paper I.

If sufficient H_2 forms within the protogalaxy, it will begin to self-shield, reducing the effective photodissociation rate. An exact treatment of the effects of self-shielding is computationally infeasible, as it would require us to solve for the full spatial, angular, and frequency dependence of the radiation field at every time step. Instead, we have chosen to incorporate it in an approximate manner. We assume that the dominant contribution to the self-shielding at a given point in the protogalaxy comes from gas close to that point, and so we only include the contribution to the self-shielding that comes from nearby H_2 .

Finally, we assume that ionization from X-rays or cosmic rays is negligible. Previous work suggests that even if a low level of ionization from such sources is present, it will not have a major effect on the outcome of the collapse (Glover & Brand 2003; Machacek et al. 2003). In any case, the initial fractional ionization in our simulations is very much higher than could be produced by a realistic flux of X-rays or cosmic rays.

A second major modification that we have made to the GADGET code is a treatment of radiative heating and cooling. In primordial gas, we include cooling from three main sources: electron impact excitation of atomic hydrogen ($\text{Ly}\alpha$ cooling), which is effective only above about 8000 K; rotational and vibrational excitation of H_2 ; and Compton cooling. Rates for $\text{Ly}\alpha$ cooling and Compton cooling were taken from Cen (1992), while for H_2 rovibrational cooling we used a cooling function from Le Bourlot et al. (1999). A number of different parameterizations of the H_2 cooling function have been used in the astrophysical literature, and so we show for reference in Figure 1 how the Le Bourlot et al. (1999) rate compares with various of the other rates.

In addition, in cases where the gas is metal enriched, we compute the amount of fine structure cooling coming from C, C^+ , O, Si, and Si^+ . In this calculation, we include the effect of excitation of the fine-structure lines by the CMB, which prevents the gas from cooling below T_{CMB} . We also include heating from H_2 photodissociation, following Black & Dalgarno (1977), and from the ultraviolet pumping of H_2 , following Burton et al. (1990).

We do not include cooling from HD, as this is only significant compared to H_2 at temperatures below $T \sim 200$ K. Dense gas which reaches these temperatures in our simulations is very soon thereafter accreted by a sink particle, at which point its further temperature evolution cannot be followed. We therefore do not expect that the lack of HD cooling in our models will significantly affect our conclusions. We also omit cooling from other primordial molecules and molecular ions (e.g. LiH and H_3^+), as these are unimportant at the densities and temperatures encountered in our simulations. Heavy molecules such as CO are also omitted, as they form in significant abundances only at densities greater than those considered in this paper, as has already been discussed at length in Paper I. A brief list of the thermal processes included in our simulations is given in Table 3; further details, in particular of our treatment of fine-structure cooling, can be found in Paper I.

2.3. Initial Conditions

2.3.1. Initial temperature and density distribution

We initialize each of our simulations with gas that is hot ($T_g = 10^4$ K) and fully ionized. The physical situation that these initial conditions are intended to represent is a protogalaxy forming within what Oh & Haiman (2003) term a ‘fossil’ H II region, an H II region surrounding an ionizing source that has switched off, containing gas that has not yet had time to cool and recombine. Prior to cosmological reionization, such regions should be relatively common, since the characteristic lifetime of the likely ionizing sources – massive Population III stars and/or active galactic nuclei – are significantly shorter than the Hubble time.

The initial temperature of gas in such a fossil H II region should, strictly speaking, depend on various factors such as the spectrum and strength of the ionizing source and the density of the gas. However, since the gas cools rapidly through $\text{Ly}\alpha$ cooling at the start of our simulations, and since the temperature at which $\text{Ly}\alpha$ cooling becomes ineffective does not depend on the initial temperature of the gas, we do not expect our results to be sensitive to small changes in the initial value of T_g .

For our purposes, we do not need to follow the assembly history of the dark matter halo in which the protogalaxy resides, or to study the response of the dark matter halo to the cooling of the gas. Therefore, we choose to model the influence of the dark matter halo (hereafter simply the ‘halo’) by using a fixed background potential. To construct this potential, we assume that the halo is spherically symmetric, with the density profile of Navarro et al. (1997):

$$\rho_{\text{dm}}(r) = \frac{\delta_c \rho_{\text{crit}}}{r/r_s (1 + r/r_s)^2}, \quad (1)$$

where r_s is a scale radius, δ_c is a characteristic (dimensionless) density, and $\rho_{\text{crit}} = 3H^2/8\pi G$ is the critical density for closure. Note that we use a value for the Hubble constant of $H_0 = 72 \text{ km s}^{-1} \text{ Mpc}^{-1}$ (Spergel et al. 2003). Following Navarro et al. (1997), we calculate the characteristic density and the scale radius from a given redshift and dark halo mass. We truncate the halo at the radius at which the value of ρ_{dm} given by equation 1 equals the cosmological background density at the beginning of the simulation. To simplify the discussion of our simulation results, we take as a fiducial example a halo with a total mass $M_{\text{tot}} = 7.8 \times 10^5 M_\odot$ and an initial redshift $z_i = 25$. For this example halo, the virial temperature $T_{\text{vir}} = 1900 \text{ K}$, the virial radius $r_{\text{vir}} = 0.1 \text{ kpc}$, and the truncation radius $r_t = 0.49 \text{ kpc}$, where both radii are given in physical units. The scale radius r_s of this example halo is 29 pc , and the full computational volume is a box of side length 1 kpc . In addition to this fiducial example, we also studied cooling and collapse in halos with various different masses in the range $4.0 \times 10^4 M_\odot < M_{\text{tot}} < 1.2 \times 10^7 M_\odot$, at redshifts in the range $20 < z < 30$. A complete list of runs is given in Table 4.

We use periodic boundary conditions for the hydrodynamic part of the force calculations to keep the gas bound within the computational volume. The self-gravity of the gas and the gravitational force exerted by the dark matter potential are not calculated periodically, since we assume that other dark matter halos and their gas content are distant enough to neglect their gravitational influence.

As we are dealing with a gravitationally bound system (the dark matter halo) that has decoupled from the Hubble flow, we do not include the effects of cosmological expansion, and we perform our simulations using physical rather than co-moving coordinates. This simplification should be reasonably accurate for gas within the virial radius of the halo, although it will break down at larger radii. However, the behaviour of the gas at radii $r \gg r_{\text{vir}}$ will have little effect on the evolution of the gas in the central regions of the halo, and since it is the latter that we are primarily concerned with in this paper, this simplification should be adequate for our current purposes.

We begin our simulations with a uniform distribution of gas with an initial density ρ_g , taken to be equal to the cosmological background density, and then allow the gas to relax isothermally until it reaches hydrostatic equilibrium. Note that this initial phase of the simulation is merely a convenient way of generating the appropriate initial conditions for the simulation proper, and so we do not include the effects of chemical evolution or cooling during this phase. The mass of gas present in our simulation was taken to be a fraction $\Omega_b/\Omega_{\text{dm}}$ of the total mass of dark matter, where the dark matter density $\Omega_{\text{dm}} = \Omega_m - \Omega_b$, and where Ω_b is the baryon density and Ω_m is the matter density. We take values for the cosmological parameters from Spergel et al. (2003) of $\Omega_b = 0.047$ and $\Omega_m = 0.29$, giving us

a total gas mass of $M_g = 0.19 M_{\text{dm}}$. Here, M_{dm} is the sum of the halo mass and the mass of the dark matter background in the simulated volume. For our fiducial example, and for our example, $M_{\text{dm}} = 1.84 \times 10^6 M_\odot$. Therefore, in this case $M_g = 3.5 \times 10^5 M_\odot$. The number of SPH particles used to represent the gas depends on the mass of the halo. We selected an appropriate particle number and particle mass by requiring that the number of particles used, N , and the particle mass, M_{part} , satisfied $N \geq 10^5$ and $M_{\text{part}} \leq 5.0 M_\odot$ respectively. Our SPH smoothing kernel encompasses approximately 40 particles and since we need twice this number in order to properly resolve gravitationally bound objects (Bate & Burkert 1997), our mass resolution, in the worst case, is $M_{\text{res}} \simeq 80 m_{\text{part}} = 400 M_\odot$. In some of the smaller halos we simulate, our mass resolution is significantly better. The values of N and M_{part} used for each of the different halo masses are summarized in Table 5, along with the corresponding values of M_{res} and also the virial temperatures of the various halos.

At our sink creation density, M_J exceeds M_{res} as long as $T > 30 \text{ K}$. This temperature is much smaller than that reached by the gas in our simulations, and so we always satisfy the Bate & Burkert (1997) resolution criterion by a comfortable margin in gas which has not been accreted by a sink.

2.3.2. *Metallicity*

We studied the evolution both of zero-metallicity, primordial gas and of metal-enriched gas. The range of metallicities studied was $10^{-3} < Z/Z_\odot < 1.0$. The value used in any particular simulation is summarized in Table 4. In particular, we performed a large number of simulations with $Z = 10^{-3} Z_\odot$. This value is an upper limit derived from QSO absorption-line studies of the low column density Ly α forest at $z \sim 3$ (Pettini 1999). Estimates of the globally-averaged metallicity produced by the sources responsible for reionization are also typically of the order of $10^{-3} Z_\odot$ (see e.g. Ricotti & Ostriker 2004). Moreover, the fact that several hundred stars with $[\text{Fe}/\text{H}] < -3$ have been observed in the Galactic halo provides solid evidence that solar mass stars can form at this metallicity (Christlieb 2003). We originally intended to examine the behaviour of the gas at even lower metallicities, but these additional simulations were rendered unnecessary by the fact that even at $Z = 10^{-3} Z_\odot$ metal cooling proved to be of no importance at the low gas densities studied in this paper.

In our simulations of metal-enriched gas, we assume that mixing is efficient and that the metals are spread out uniformly throughout the computational domain. We also assume that the relative abundances of the various metals in the enriched gas are the same as in solar metallicity gas; given the wide scatter that exists in observational determinations and theoretical predictions of abundance ratios in very low-metallicity gas, this seems to us to

be the most conservative assumption. However, variations in the relative abundances of an order of magnitude or less will not significantly alter our results.

As we discuss in Paper I, substantial uncertainties exist concerning the presence, abundance, size distribution, and composition of dust grains in low-metallicity gas at high redshift. An exhaustive examination of the various possibilities would require an unfeasibly large number of simulations to be performed, and so we instead make the simplifying assumption that if dust is present, it has similar properties to Milky Way dust, but with an abundance that is a factor of Z/Z_\odot smaller than the Galactic value. To allow us to investigate the relative importance of the dust and the gas-phase metals, we perform simulations both with and without dust.

2.3.3. Other details

We also investigate the influence of a UV background. By $z = 25$, a considerable UV background may already have developed (Haiman et al. 2000; Glover & Brand 2003), particularly if cosmological reionization occurs at a redshift near the upper end of the range suggested by the *WMAP* polarization results (Spergel et al. 2007). To explore how the presence of a UV background will influence our conclusions, we have run simulations with UV field strengths of $J_{21} = 0.01$ and 0.1 , as well as with no background present.

Simulations were run for ~ 1 Hubble time, t_H , which at $z = 25$ corresponds to about 100 Myr. At times $t > t_H$, individual dark matter halos can no longer be treated as isolated objects, since most halos will have undergone at least one major merger or interaction by this time. For our fiducial halo, the free-fall time $t_{\text{ff}} \sim (G\rho)^{-1/2}$ varies between 4 Myr near the central cusp and 450 Myr in the outer envelope.

For ease of reference, we have given the runs discussed in the following sections simple alphanumeric identifiers. We have (arbitrarily) divided up our model halos into three size classes: “small” halos, with masses $M < 10^5 M_\odot$; “intermediate” halos, with $10^5 < M < 4.5 \times 10^6 M_\odot$; and “large” halos with $M > 4.5 \times 10^6 M_\odot$. The first character of the identifier indicates with which of these classes the run in question is associated: “S” denotes a small halo, “I” an intermediate halo, and “L” a large halo. The next two digits in the identifier denote the initial redshift of the simulation. Next, there follows a character denoting the metallicity: “Z” corresponds to zero metallicity, while “L,” “M,” “N,” and “S” correspond to metallicities 10^{-3} , 10^{-2} , 10^{-1} , and $1 Z_\odot$, respectively. Following this is a number denoting the strength of the UV background: 1 corresponds to no background, while 2 and 3 correspond to $J_{21} = 0.01$ and 0.1 , respectively. Finally, runs in which dust is included have a “D”

appended. To give an example: run I25-M3D is a run performed at redshift $z = 25$ with an intermediate-sized halo that has a metallicity $Z = 10^{-2} Z_{\odot}$, an ultraviolet background field strength of $J_{21} = 0.1$, and that includes the effects of dust.

3. Results

3.1. Zero-Metallicity Gas

Before examining the behaviour of the metal-enriched gas, it is prudent to first examine what happens in the absence of metals, i.e. in gas of wholly primordial composition. Previous work suggests that there is a critical protogalactic mass M_{crit} such that gas in protogalaxies with $M > M_{\text{crit}}$ is able to cool and collapse within a Hubble time, while gas in protogalaxies with $M < M_{\text{crit}}$ cannot (see e.g. Tegmark et al. 1997; Machacek et al. 2001; Yoshida et al. 2003; Mashchenko et al. 2006; O’Shea & Norman 2007).

To verify that we recover the same behaviour, we performed a set of three runs at $z = 30$ with halo masses spanning a range of 2 orders of magnitude. The halos in these three runs, which we designate as S30-Z1, I30-Z1, and L30-Z1, had masses of $4.0 \times 10^4 M_{\odot}$, $4.8 \times 10^5 M_{\odot}$ and $4.8 \times 10^6 M_{\odot}$ respectively. In Figure 2, we show the time evolution of the mean number density and mean temperature within the scale radius r_s in these runs.

Table 6 gives the properties of the gas within the scale radius after 100 Myr of evolution. The table lists the minimum central temperature $T_{c,\text{min}}$ and the maximum central density $n_{c,\text{max}}$. We also calculate the fractional H_2 abundance with respect to the total number of hydrogen nuclei, and list the maximum central value, $x_{\text{H}_2,c,\text{max}}$, in the table.

The mass fraction of gas within a sink particle is denoted by f_{sink} . Because we have no information on the density and temperature distribution within the sink particle radius, we adopt the values at time of sink particle formation in Table 6. Note that as the gas in run S30-Z1 does not collapse, it never reaches the density required for a sink particle to form.

Both Figure 2 and Table 6 clearly demonstrate the change in behaviour that occurs for increasing M : gas in run L30-Z1 cools and collapses very quickly, on a timescale $t \ll t_{\text{H}}$, while gas in run I30-Z1 cools and collapses on a slower timescale $t \sim t_{\text{H}}$. Finally, the gas in run S30-Z1 cools, but not by enough to bring its temperature below the halo virial temperature, and so it does not collapse within a Hubble time. Indeed, we have run this simulation for ~ 520 Myr longer than is shown in the plot, but find no evidence for collapse even after this extended period. We can therefore conclude that $4.0 \times 10^4 M_{\odot} < M_{\text{crit}} < 4.8 \times 10^5 M_{\odot}$, with the value likely somewhere near the upper end of this range. For comparison, Tegmark et al.

(1997) find that $M_{\text{crit}} = 10^6 M_{\odot}$ at $z = 30$; Machacek et al. (2001) find a significantly smaller value of $M_{\text{crit}} = 1.25 \times 10^5 M_{\odot}$ at the same redshift; and Yoshida et al. (2003) find that $M_{\text{crit}} \simeq 7.0 \times 10^5 M_{\odot}$ at $z < 25$. More recently, O’Shea & Norman (2007) have shown that in their ensemble of simulations of primordial star formation, the mass of the first star-forming halo lies in the range $1.4 \times 10^5 < M < 6.9 \times 10^5 M_{\odot}$, where the scatter appears to be a result of the sensitivity of the problem to the initial conditions. Our own estimate of M_{crit} is in general agreement with these determinations, suggesting that our basic treatment of the physics of the primordial gas is sound.

Another area that we can explore with our zero-metallicity runs is the response of the gas to the presence of an ultraviolet background. Previous work has shown that H_2 cooling of protogalactic gas is significantly affected once the strength of the background exceeds $J_{21} \simeq 0.01$ and that collapse in small halos is almost entirely suppressed for $J_{21} \geq 0.1$, owing to efficient photodissociation of the H_2 (Haiman et al. 2000; Machacek et al. 2001; Yoshida et al. 2003; Mashchenko et al. 2006). We show in Figure 3 an example of what happens in our own simulations as the strength of the background is increased. In the figure, we plot results from three runs performed at $z = 25$ with halo mass $M = 7.8 \times 10^5 M_{\odot}$. These runs are designated I25-Z1, I25-Z2, and I25-Z3 and had UV background field strengths of $J_{21} = 0.0, 0.01$ and 0.1 , respectively. We see from the figure that the imposed UV background of strength $J_{21} = 0.01$ in run I25-Z2 delays collapse by more than 30 Myr compared to run I25-Z1, but that collapse does eventually occur. On the other hand, a further increase in the UV background field strength by a factor of 10 completely inhibits the collapse of the gas within the time frame of our simulation. These results are in good agreement with the previous studies cited above, further increasing our confidence that our basic modelling is sound.

3.2. Metal-Enriched Gas

3.2.1. Low-Metallicity Protogalaxies

Having established how primordial gas behaves in these conditions, we next examined the effect of enriching the gas with metals. As previously mentioned in § 2.3, we focussed initially on gas with a metallicity $Z = 10^{-3} Z_{\odot}$. This metallicity is at the upper limit of the range of values proposed for the so-called critical metallicity Z_{crit} , the value of the metallicity at which efficient fragmentation and low-mass star formation is hypothesized to first occur (Bromm et al. 2001; Bromm & Loeb 2003; Schneider et al. 2002; Omukai et al. 2005). It is also comparable to the globally averaged metallicity produced by the sources responsible for reionization (see e.g. Ricotti & Ostriker 2004).

In the top panel of Figure 4 we show the time evolution of the relative difference between the central density in run I25-L1 and in I25-Z1. In other words, we plot $|n_{Z,c} - n_{L,c}|/n_{Z,c}$, where $n_{L,c}$ and $n_{Z,c}$ are the central densities in runs I25-L1 and I25-Z1, respectively. We plot this quantity to highlight the difference between the two runs, which would be difficult to discern in a more conventional comparison plot. We see that prior to sink particle formation, the central density of the two runs differs by less than 10%, and that at early times ($t < 50$ Myr), the difference is less than 1%. In the bottom panel of Figure 4 we show a similar plot for the central temperature in the two runs. Again, the difference between the two runs is very small.

These results demonstrate that the cooling of the gas at low densities ($n < 1 \text{ cm}^{-3}$) and high temperatures ($T > 2000 \text{ K}$) is barely influenced by the presence of metals: fine-structure cooling contributes only marginally to the total cooling rate, and the results of the runs agree to within 1%. The evolution of cooling during the first 50 Myr and the onset of collapse are thus almost independent of the metallicity of the gas, at least for gas with $Z \leq 10^{-3} Z_{\odot}$. At later times during the collapse, the difference between the metal-enriched and the zero-metallicity models becomes more pronounced, indicating that metal-line cooling is beginning to play a more significant role. Despite this, the behaviour of the gas in the two runs remains very similar up to the point at which sink formation occurs (i.e. at $n \leq 500 \text{ cm}^{-3}$).

An obvious question to ask is whether these results are somehow peculiar to the particular combination of halo mass and redshift that we have chosen to examine. To investigate this, we performed additional simulations with both $Z = 0$ and $10^{-3} Z_{\odot}$ for a range of different halo masses and redshifts, as summarized in Table 4. We found that in all cases we obtained similar results; the thermal and dynamical evolution of gas in runs with $Z = 10^{-3} Z_{\odot}$ differed very little from that of gas in runs with $Z = 0$.

3.2.2. The effects of rotation

We have also investigated the possibility that our results were significantly affected by our neglect of the effects of rotation in the majority of our runs. Theoretically, we do not expect rotation to be important on scales $r \gg \lambda r_{\text{vir}}$, where λ is the dimensionless spin parameter, given by (Peebles 1971)

$$\lambda = \frac{J|E|^{1/2}}{GM^{5/2}}, \quad (2)$$

where J is the total angular momentum of the halo, M is the halo mass and E is the total (kinetic plus potential) energy of the halo. Previous work has shown that for halos with the range of masses and redshifts considered in this paper, λ has a lognormal distribution,

with mean $\bar{\lambda} = 0.035$ (Yoshida et al. 2003). Therefore, we expect that rotation will only significantly affect the dynamics of the gas within the innermost few percent of the halo. As this is typically comparable to the radius at which we cease to be able to resolve the collapse of the gas, we do not expect the inclusion of rotation to significantly affect our results or to materially alter our conclusions.

In order to verify that this is a reasonable expectation, we performed one simulation in which the initial gas distribution was given a non-zero angular momentum. Within the virial radius of the halo, the gas was placed into rotation with constant angular velocity. At larger radii, the initial angular velocity decreased linearly with radius, reaching zero at the truncation radius of the halo. This run, which we designate hereafter as I25-Z1-ROT, had a spin parameter $\lambda = 0.05$. The other parameters used for this run were the same as in run I25-Z1. In Figure 5, we compare the outcome of these two simulations. We see that, as expected, rotation has very little effect on the evolution of the gas at early times. It does appear to affect the evolution once the density exceeds $n = 100 \text{ cm}^{-3}$, significantly slowing the collapse, but at this point we are close to the resolution limit of our simulation and so we are unable to say with any certainty whether or not a rotationally supported disk forms. Nevertheless, as the main results of this paper concern the evolution of the gas at densities $n \ll 100 \text{ cm}^{-3}$, it is clear that they are unaffected by our neglect of rotation in the majority of our simulations.

3.2.3. When Do Metals Make a Difference?

If cooling from metals is ineffective when $Z = 10^{-3} Z_{\odot}$, then just when does it become important? How enriched does the gas need to be before metal-line cooling makes a significant difference? To investigate this, we performed a set of additional runs using our fiducial halo parameters ($z = 25$, $M = 7.8 \times 10^5 M_{\odot}$) that looked at the effects of further increasing Z . In Figure 6, we plot the time evolution of the central density and central temperature in runs I25-Z1, I25-L1, I25-M1, I25-N1, and I25-S1, which had metallicities of $Z = 0.0, 10^{-3}, 10^{-2}, 0.1$ and $1.0 Z_{\odot}$, respectively. We also show in the plot the results of runs I25-L1D, I25-M1D, and I25-S1D, which had metallicities of $Z = 10^{-3}, 10^{-2}$ and $1.0 Z_{\odot}$, respectively, and which differed from runs I25-L1, I25-M1, and I25-S1 by including the chemical and thermal effects of dust.

It is clear from the figure that all of the runs with $Z \leq 0.01 Z_{\odot}$ evolve in essentially the same way. Some minor differences in the rate of collapse and in the central temperature of the gas are apparent at late times, particularly in the two runs with $Z = 0.01 Z_{\odot}$, but these do not appear likely to significantly affect the outcome of the simulation. If we enrich

the gas by another order of magnitude, to $Z = 0.1 Z_{\odot}$, however, then we begin to see the metals playing a significant role in the cooling of the gas. In run I25-N1 the gas cools more rapidly than in any of the lower metallicity runs, and as a consequence, runaway gravitational collapse sets in approximately 10 Myr earlier than in the lower metallicity runs. Nevertheless, the evolution of the gas in this run remains qualitatively very similar to that in the lower metallicity runs. It is only when we enrich the gas by a further order of magnitude, to solar metallicity, that we see a truly dramatic difference in the outcome of the simulation, with the gas in runs I25-S1 and I25-S1D cooling and collapsing within the first 20 Myr of the run. Based on these results, we would estimate the critical metallicity at which metal cooling dominates in the low-density gas to be $Z_{\text{crit}} \sim 0.1 Z_{\odot}$, to the nearest order of magnitude.

Figure 6 also allows us to assess the role played by dust in these systems. The fact that runs I25-L1D and I25-M1D produce essentially identical results to runs I25-L1 and I25-M1 demonstrates that at $Z = 0.01 Z_{\odot}$ and below, dust has a minimal effect on the low-density evolution of these systems. On the other hand, at high metallicities, dust *does* significantly affect the evolution of the gas. Although the presence of dust might be expected to aid the cooling of the gas, it is clear from Figure 6 that in actual fact the gas cools more rapidly when dust is not present. This appears to be a consequence of the fact that the ionized gas recombines more rapidly when dust is present, owing to recombination of ionized hydrogen on the surface of dust grains, with the result that both the Compton cooling rate, as well as the contributions of electron-ion and electron-atom collisions to the fine-structure cooling rate, fall off more rapidly with time.

3.2.4. Collapse with a UV background

Finally, it is important to determine whether metal-line cooling allows collapse to occur in UV-irradiated halos that would otherwise be unable to collapse. Figure 7 summarizes the results of a set of simulations designed to address this question. It shows the evolution of the central density and temperature of the gas in a set of runs in which $J_{21} = 0.1$, M and z were held constant at their fiducial values, and the metallicity was varied. Details of the eventual state of the gas at the end of these runs are given in Table 6. We see that even at metallicities as high as $Z = 0.01 Z_{\odot}$, an ultraviolet background flux of strength $J_{21} = 0.1$ is sufficient to completely suppress collapse. We therefore conclude that *in low-metallicity, low-mass protogalactic halos, metal-line cooling cannot initiate collapse*. Either the surviving H_2 provides enough cooling to allow collapse to occur, irrespective of whether or not there are metals present, or the gas does *not* collapse. Only at quite high metallicities ($Z \geq 0.1 Z_{\odot}$) do the metals actually make an appreciable difference to the evolution of the gas.

4. Discussion

At first sight, the fact that fine structure cooling from metals has little impact on the thermal or dynamical evolution of the gas at metallicities below $0.1 Z_{\odot}$ is somewhat surprising, given that Bromm et al. (2001) found that gas with a metallicity of only $Z = 10^{-3} Z_{\odot}$ could cool rapidly and fragment even in the complete absence of molecular hydrogen. However, comparison of the cooling time due to fine-structure emission with the free-fall time of the gas helps to make the situation clear. The cooling time due to fine-structure emission is given by

$$t_{\text{cool,fs}} = \frac{1}{\gamma - 1} \frac{nkT}{\Lambda_{\text{fs}}}, \quad (3)$$

where Λ_{fs} is the total cooling rate per unit volume due to fine-structure emission, T is the temperature of the gas, γ is the adiabatic index, n is the number density of the gas, and k is the Boltzmann constant. The free-fall time can be written as

$$t_{\text{ff}} = \left(\frac{3\pi}{32G\rho} \right)^{1/2}, \quad (4)$$

where G is the gravitational constant and $\rho = \rho_{\text{gas}} + \rho_{\text{dm}}$. The gas density ρ_{gas} can be written in terms of the number density n as $\rho_{\text{gas}} = \mu n$, where μ is the mean molecular weight of the gas.

In Figure 8, we indicate the temperatures and densities at which $t_{\text{cool,fs}} = t_{\text{ff}}$ for $10^{-3} Z_{\odot}$ gas, for three different assumed fractional ionizations, with $x_e = 1.0$ (fully ionized gas), 10^{-2} , and 10^{-4} . In each case, we assume that the carbon and silicon are present only as C^+ or Si^+ , since a fairly small external UV flux is sufficient to achieve this. In the $x_e = 1.0$ case, we also assume that all of the oxygen is O^+ , since charge transfer between oxygen and hydrogen, which have nearly identical ionization potentials, ensures that $x_{\text{O}^+}/x_{\text{O}} \simeq x_{\text{H}^+}/x_{\text{H}}$. For the dark matter density ρ_{dm} we adopt the value found at the center of our fiducial protogalactic halo at $t=0$, $\rho_{\text{dm}} \simeq 8 \times 10^{-22} \text{g cm}^{-3}$. In the plot, regions to the left of the line have $t_{\text{cool,fs}} > t_{\text{ff}}$, while those to the right have $t_{\text{cool,fs}} < t_{\text{ff}}$.

At the beginning of our fiducial simulation, gas in the center of the halo has a temperature $T = 10^4 \text{ K}$ and a number density $n = 0.03 \text{ cm}^{-3}$. It therefore lies outside of the regime where fine-structure cooling is efficient, and so it is not surprising that we find that metal-line cooling is initially unimportant. As the gas cools, whether through Compton cooling or H_2 emission, and begins to compress as it falls into the halo, it moves towards the temperature and density regime in which fine-structure cooling is effective. As an example, we plot in Figure 8 the trajectory in the density-temperature plane followed by gas at the center of the halo in run I25-L1. However, at the same time as the gas is cooling and collapsing, it is also recombining. This causes the boundary of the efficient cooling regime to move to the

right of the plot, towards higher densities. The physical reason for this shift is the fact that free electrons are much more effective than neutral hydrogen at exciting the C^+ and Si^+ fine-structure lines, and so electron excitation dominates for $x_e > 10^{-2}$ – 10^{-3} , depending on the temperature. The net effect is that fine-structure cooling remains of little importance until the gas is near the high-cooling regime. This only happens after considerable cooling and compression has already taken place, and therefore does not occur at all if H_2 cooling is ineffective, as is the case, for instance, in runs I25-Z3 or I25-L3.

For gas with a metallicity greater than $10^{-3} Z_\odot$, fine-structure cooling is effective in a larger region of the density-temperature plane. At low densities ($n < 1 \text{ cm}^{-3}$), an increase in Z of an order of magnitude shifts the solid lines in Figure 8 by an order of magnitude with respect to density. This allows us to estimate the metallicity at which fine-structure cooling will dominate even in the initial low-density gas. We find that fine-structure cooling should dominate for metallicities in excess of 0.1 – $1.0 Z_\odot$, depending on the details of the evolutionary trajectory followed by the gas at early times. This estimate agrees well with the results we obtain from our SPH simulations.

Changes to the halo mass or redshift of collapse will affect this estimate in two ways. First, increasing the redshift of collapse will make the dark matter halo denser and will therefore decrease t_{ff} at early times, when dark matter is gravitationally dominant. This will shrink the region in which fine-structure cooling can effectively operate. Second, altering the halo mass and redshift will alter the evolutionary trajectory followed by the gas. Specifically, since the initial temperature of the gas is fixed at 10^4 K in these simulations, changes in M or z that increase the virial temperature of the halo will make the gas more gravitationally unstable, allowing it to collapse more quickly. The collapsing gas will therefore be hotter than in our fiducial case (as it will have had less time to cool), and will also be slightly more ionized. On the other hand, if the virial temperature of the halo is lowered, then the gas will be more stable, will collapse more slowly, and will therefore be cooler and less ionized than in our fiducial case. However, in either case, we would not expect to see a change of more than a factor of a few in the critical metallicity required for effective fine-structure cooling at low densities, and our estimate should therefore still be of the correct order of magnitude.

Given these results, we next ask whether they can possibly be consistent with the results of Bromm et al. (2001), who find that in their simulations, fine structure cooling is effective even for $Z = 10^{-3} Z_\odot$, which is at least 2 orders of magnitude smaller than our value. In fact, their results do actually appear to be consistent with ours, despite the apparent disagreement. The reason is due to the difference in the initial conditions used for their simulations and for ours. The gas in their simulations has an initial temperature of 200 K at $z = 100$, and its temperature falls further due to adiabatic cooling in the IGM prior to the formation of

their simulated protogalactic halo at $z \sim 30$. Since this halo has a mass of $2 \times 10^6 M_\odot$ and a virial temperature $T_{\text{vir}} \simeq 5000$ K, the temperature of the gas at the moment at which the halo forms is very much smaller than the halo virial temperature. Consequently, thermal pressure is initially unable to prevent the collapse of gas into the halo. As it collapses, the gas heats up, and the thermal pressure eventually becomes large enough to halt the collapse. However, this does not occur until the gas temperature is approximately equal to the halo virial temperature, by which time the gas density has increased to a value $n \simeq 300 \text{ cm}^{-3}$. As can be seen from Figure 8, gas with this density and with a temperature of 5000 K lies close to or within the regime where $t_{\text{cool,fs}} < t_{\text{ff}}$ (depending on its fractional ionization), and so it is not surprising that Bromm et al. (2001) find that fine-structure cooling is effective and that the gas can cool even in the complete absence of H_2 . It is also important to stress that Bromm et al. (2001) do not find fine-structure cooling to be important at densities $n \ll 100 \text{ cm}^{-3}$, as the almost adiabatic initial evolution of the gas makes clear.

For comparison, our simulations start with a high initial gas temperature of 10^4 K and involve halos with virial temperatures $T_{\text{vir}} < 10^4$ K; for instance, $T_{\text{vir}} \simeq 1900$ K in our fiducial simulation. This means that in our simulations, $T_{\text{gas}} > T_{\text{vir}}$ initially, with the result that thermal pressure support is important right from the start. Indeed, at the beginning of our simulations pressure precisely balances gravity, by design. Therefore, there is no initial phase of pure free-fall collapse as in the Bromm et al. (2001) simulations. Instead, significant gravitational contraction occurs only if the gas is able to cool to a temperature of order T_{vir} or below, which, since fine-structure cooling is initially ineffective, will only occur if enough H_2 can form in the low-density gas. At late times in our simulations, we would expect to see fine-structure cooling become more effective at lower Z , in line with what Bromm et al. (2001) find, but unfortunately the required gas density is only marginally resolvable with our current simulations.

While the two sets of simulations therefore appear to be consistent with each other, a key question is obviously which set of initial conditions is more appropriate for describing the early evolution of small, metal enriched protogalaxies. We argue that it is difficult to see how intergalactic gas could become metal enriched without at some point being ionized. Previous calculations have shown that the size of a typical region enriched by a Population III supernova is much smaller than the size of the H II region created by its progenitor star (see e.g. Bromm et al. 2003). We would therefore expect our initial conditions to be more appropriate than those of Bromm et al. (2001) for treating recently enriched and ionized regions. However, if enough time elapses following the enrichment event for the gas to be able to cool down to a temperature of a few hundred K, then the Bromm et al. (2001) initial conditions will be more appropriate. As Oh & Haiman (2003) show, this is most likely to occur in high-redshift gas with a low overdensity. Then Compton cooling is fast and highly

effective and can cool the gas to $T \sim 300$ K within a recombination time. On the other hand, at lower redshifts, or at higher overdensities, the gas recombines faster than it cools, and the temperature that can be reached by Compton cooling alone is much higher. This is the case in our simulated halos. Note that in either case the metals play no significant role in determining whether or not the gas is able to collapse.

An important implication of these results is that if we are primarily concerned with investigating questions such as how M_{crit} evolves with redshift, or how UV feedback in the form of Lyman-Werner photons affects the ability of the gas to cool, then we need not worry about the effects of metal enrichment. This is because the thermal evolution of the gas on the scales of interest for these questions is completely dominated by Compton cooling and/or H_2 cooling. Therefore, results from studies such as Haiman et al. (2000) or Yoshida et al. (2003) give a better guide to the behaviour of small, low-metallicity protogalaxies than might have been anticipated (although the additional complications posed by the mechanical energy injected into the gas by H II regions and supernovae do of course still need to be taken into account).

Finally, it is important to stress that our results do not address the question of whether or not there is a critical metallicity Z_{crit} above which fine structure cooling from metals allows efficient fragmentation to occur. This is because if fragmentation does occur, we would expect it to occur at densities $n > 500 \text{ cm}^{-3}$, which are unresolved in our current simulations. We will examine this question with much higher resolution simulations in a future paper.

We thank Z. Haiman and S. Kitsionas for useful discussions. We also thank the anonymous referee for his report, which helped us to greatly improve the presentation of this paper. R. S. K. and A. K. J. acknowledge support from the Emmy Noether Program of the Deutsche Forschungsgemeinschaft (grant KL1358/1). M.-M. M. L. and S. C. O. G. acknowledge support from NSF grants AST99-85392 and AST03-07793 and NASA grants NAG5-10103 and NAG5-13028. The simulations discussed in this paper were performed on the PC cluster “sanssouci” at the Astrophysikalisches Institut Potsdam.

REFERENCES

- Abel, T., Bryan, G. L., & Norman, M. L. 2002, *Science*, 295, 93
- Bakes, E. L. O., & Tielens, A. G. G. M. 1994, *ApJ*, 427, 822
- Bate, M. R., Bonnell, I. A., & Price, N. M. 1995, *MNRAS*, 277, 362

- Bate, M. R. & Burkert, A. 1997, MNRAS, 288, 1060
- Benz, W. 1990, in Numerical Modelling of Nonlinear Stellar Pulsations Problems and Prospects, ed. J. R. Buchler (Dordrecht: Kluwer), 269
- Black, J. H. & Dalgarno, A. 1977, ApJS, 34, 405
- Bromm, V., Coppi, P. S., & Larson, R. B. 2002, ApJ, 564, 23
- Bromm, V., Ferrara, A., Coppi, P. S., & Larson, R. B. 2001, MNRAS, 328, 969
- Bromm, V. & Larson, R. B. 2004, ARA&A, 42, 79
- Bromm, V. & Loeb, A. 2003, Nature, 425, 812
- Bromm, V., Yoshida, N., & Hernquist, L. 2003, ApJ, 596, L135
- Burton, M. G., Hollenbach, D. J., & Tielens, A. G. G. M. 1990, ApJ, 365, 620
- Cen, R. 1992, ApJS, 78, 341
- Christlieb, N. 2003, Rev. Mod. Astron., 16, 191
- Ciardi, B. & Ferrara, A. 2005, Space Sci. Rev., 116, 625
- Cojazzi, P., Bressan, A., Lucchin, F., Pantano, O., & Chavez, M. 2000, MNRAS, 315, L51
- Draine, B. T., & Bertoldi, F. 1996, ApJ, 468, 269
- Dunn, G. H. 1968, Phys. Rev., 172, 1
- Ferland, G. J., Peterson, B. M., Horne, K., Welsh, W. F., & Nahar, S. N. 1992, ApJ, 387, 95
- Galli, D., & Palla, F. 1998, A&A, 335, 403
- Glover, S. C. O. 2005, Space Sci. Rev., 117, 445
- Glover, S. C. O. & Brand, P. W. J. L. 2001, MNRAS, 321, 385
- Glover, S. C. O. & Brand, P. W. J. L. 2003, MNRAS, 340, 210
- Glover, S. C. O., Jappsen, A.-K., 2007, ApJ, submitted. (Paper I).
- Haiman, Z., Abel, T., & Rees, M. J. 2000, ApJ, 534, 11
- Hollenbach, D., & McKee, C. F. 1979, ApJS, 41, 555

- Hollenbach, D., & McKee, C. F. 1989, *ApJ*, 342, 306
- Janev, R. K., Langer, W. D., Evans, K., & Post, D. E. 1987, *Elementary Processes in Hydrogen-Helium Plasmas*, Springer
- Jappsen, A.-K., Klessen, R. S., Larson, R. B., Li, Y., & Mac Low, M.-M. 2005, *A&A*, 435, 611
- Johnson, J. L., Greif, T. H. & Bromm, V. 2007, *APJ*, submitted, (astro-ph/0612254)
- Karpas, Z., Anicich, V., & Huntress, W. T. 1979, *J. Chem. Phys.*, 70, 2877
- Kingdon, J. B. & Ferland, G. J. 1996, *ApJS*, 106, 205
- Launay, J. M., Le Dourneuf, M., & Zeippen, C. J. 1991, *A&A*, 252, 842
- Le Bourlot, J., Pineau des Forêts, G., & Flower, D. R. 1999, *MNRAS*, 305, 802
- Lepp, S., & Shull, J. M. 1983, *ApJ*, 270, 578
- Le Teuff, Y. H., Millar, T. J., & Markwick, A. J. 2000, *A&AS*, 146, 157
- Mac Low, M.-M., & Shull, J. M. 1986, *ApJ*, 302, 585
- Machacek, M. E., Bryan, G. L., & Abel, T. 2001, *ApJ*, 548, 509
- Machacek, M. E., Bryan, G. L., & Abel, T. 2003, *MNRAS*, 338, 273
- Martin, P. G., Keogh W. J., & Mandy, M. E. 1998, *ApJ*, 499, 793
- Mashchenko, S., Couchman, H. M. P. & Sills, A., *ApJ*, 639, 633
- Matsuda, T., Satō, H., & Takeda, H. 1969, *Prog. Th. Phys.*, 42, 219
- Monaghan, J. J. 1992, *ARA&A*, 30, 543
- Monaghan, J. J. 2005, *Rep. Prog. Phys.*, 68, 1703
- Moseley, J., Aberth, W., & Peterson, J. R. 1970, *Phys. Rev. Lett.*, 24, 435
- Nahar, S. N. 1999, *ApJS*, 120, 131
- Nahar, S. N. 2000, *ApJS*, 126, 537
- Nahar, S. N. & Pradhan, A. K. 1997, *ApJS*, 111, 339
- Navarro, J. F., Frenk, C. S., & White, S. D. M. 1997, *ApJ*, 490, 493

- Oh, S. P. & Haiman, Z. 2003, MNRAS, 346, 456
- Omukai, K., Tsuribe, T., Schneider, R., & Ferrara, A. 2005, ApJ, 626, 627
- O’Shea, B. W., Abel, T., Whalen, D., & Norman, M. L. 2005, ApJ, 628, L5
- O’Shea, B. W., Norman, M. L. 2007, ApJ, 654, 66
- Peebles, P. J. E. & Dicke, R. H. 1968, ApJ, 154, 891
- Peebles, P. J. E. 1971, A&A, 11, 377
- Pettini, M. 1999, in Chemical Evolution from Zero to High Redshift, eds. J. R. Walsh, M. R. Rosa, (Berlin: Springer), 233
- Poulaert, G., Brouillard, F., Claeys, W., McGowan, J. W., & Van Wassenhove, G. 1978, J. Phys. B, 11, L671
- Ramaker, D. E., & Peek, J. M. 1976, Phys. Rev. A, 13, 58
- Ricotti, M., Gnedin, N. Y., & Shull, J. M. 2002, ApJ, 575, 33
- Ricotti, M. & Ostriker, J. P. 2004, MNRAS, 350, 539
- Saslaw, W. C. & Zipoy, D. 1967, Nature, 216, 976
- Savin, D. W., Krstic, P. S., Haiman, Z., & Stancil, P. C. 2004, ApJ, 606, L167; erratum ApJ, 607, L147
- Schneider, I. F., Dulieu, O., Giusti-Suzor, A., & Roueff, E. 1994, ApJ, 424, 983; erratum ApJ, 486, 580
- Schneider, R., Ferrara, A., Natarajan, P. & Omukai, K. 2002, ApJ, 571, 30
- Spergel, D. N., Verde, L., Peiris, H. V., et al. 2003, ApJS, 148, 175
- Spergel, D. N., et al. 2007, ApJ, in press, (astro-ph/0603449)
- Springel, V., Yoshida, N., & White, S. D. M. 2001, New Astron., 6, 79
- Stancil, P. C., Havener, C. C., Krstic, P. S., Schultz, D. R., Kimura, M., Gu, J.-P., Hirsch, G., Buenker, R. J., & Zygelman, B. 1998, ApJ, 502, 1006
- Stancil, P. C., Schultz, D. R., Kimura, M., Gu, J.-P., Hirsch, G., & Buenker, R. J. 1999, A&AS, 140, 225

- Stibbe, D. T., & Tennyson, J. 1999, *ApJ*, 513, L147
- Tegmark, M., Silk, J., Rees, M. J., Blanchard, A., Abel, T., & Palla, F. 1997, *ApJ*, 474, 1
- Verner, D. A., Ferland, G. J., Korista, K. T. & Yakovlev, D. G. 1996, *ApJ*, 465, 487
- Voronov, G. S. 1997, *ADNDT*, 65, 1
- Weingartner, J. C. & Draine, B. T. 2001, *ApJ*, 563, 842
- Wishart, A. W. 1979, *MNRAS*, 187, 59P
- Wolfire, M. G., Hollenbach, D., McKee, C. F., Tielens, A. G. G. M., & Bakes, E. L. O. 1995, *ApJ*, 443, 152
- Yoshida, N., Abel, T., Hernquist, L., & Sugiyama, N. 2003, *ApJ*, 592, 645

Table 1. List of Reactions Included in Our Chemical Network

Number	Reaction	Reference
1	$\text{H} + \text{e}^- \rightarrow \text{H}^- + \gamma$	Wishart (1979)
2	$\text{H}^- + \text{H} \rightarrow \text{H}_2 + \text{e}^-$	Launay et al. (1991)
3	$\text{H} + \text{H}^+ \rightarrow \text{H}_2^+ + \gamma$	Ramaker & Peek (1976)
4	$\text{H} + \text{H}_2^+ \rightarrow \text{H}_2 + \text{H}^+$	Karpas et al. (1979)
5	$\text{H}^- + \text{H}^+ \rightarrow \text{H} + \text{H}$	Moseley et al. (1970)
6	$\text{H}_2^+ + \text{e}^- \rightarrow \text{H} + \text{H}$	Schneider et al. (1994)
7	$\text{H}_2 + \text{H}^+ \rightarrow \text{H}_2^+ + \text{H}$	Savin et al. (2004)
8	$\text{H}_2 + \text{e}^- \rightarrow \text{H} + \text{H} + \text{e}^-$	Stibbe & Tennyson (1999)
9	$\text{H}_2 + \text{H} \rightarrow \text{H} + \text{H} + \text{H}$	Mac Low & Shull (1986)
10	$\text{H}_2 + \text{H}_2 \rightarrow \text{H}_2 + \text{H} + \text{H}$	Martin et al. (1998)
11	$\text{H} + \text{e}^- \rightarrow \text{H}^+ + \text{e}^- + \text{e}^-$	Janev et al. (1987)
13	$\text{H}^+ + \text{e}^- \rightarrow \text{H} + \gamma$	Ferland et al. (1992)
15	$\text{H}^- + \text{e}^- \rightarrow \text{H} + \text{e}^- + \text{e}^-$	Janev et al. (1987)
16	$\text{H}^- + \text{H} \rightarrow \text{H} + \text{H} + \text{e}^-$	Janev et al. (1987)
17	$\text{H}^- + \text{H}^+ \rightarrow \text{H}_2^+ + \text{e}^-$	Poulaert et al. (1978)

Table 1—Continued

Number	Reaction	Reference
30	$\text{C}^+ + \text{e}^- \rightarrow \text{C} + \gamma$	Nahar & Pradhan (1997)
31	$\text{Si}^+ + \text{e}^- \rightarrow \text{Si} + \gamma$	Nahar (2000)
32	$\text{O}^+ + \text{e}^- \rightarrow \text{O} + \gamma$	Nahar (1999)
33	$\text{C} + \text{e}^- \rightarrow \text{C}^+ + \text{e}^- + \text{e}^-$	Voronov (1997)
34	$\text{Si} + \text{e}^- \rightarrow \text{Si}^+ + \text{e}^- + \text{e}^-$	Voronov (1997)
35	$\text{O} + \text{e}^- \rightarrow \text{O}^+ + \text{e}^- + \text{e}^-$	Voronov (1997)
36	$\text{O}^+ + \text{H} \rightarrow \text{O} + \text{H}^+$	Stancil et al. (1999)
37	$\text{O} + \text{H}^+ \rightarrow \text{O}^+ + \text{H}$	Stancil et al. (1999)
39	$\text{C} + \text{H}^+ \rightarrow \text{C}^+ + \text{H}$	Stancil et al. (1998)
42	$\text{Si} + \text{H}^+ \rightarrow \text{Si}^+ + \text{H}$	Kingdon & Ferland (1996)
44	$\text{C}^+ + \text{Si} \rightarrow \text{C} + \text{Si}^+$	Le Teuff et al. (2000)
51	$\text{H}^- + \gamma \rightarrow \text{H} + \text{e}^-$	Wishart (1979)
52	$\text{H}_2^+ + \gamma \rightarrow \text{H} + \text{H}^+$	Dunn (1968)
53	$\text{H}_2 + \gamma \rightarrow \text{H} + \text{H}$	Draine & Bertoldi (1996)
56	$\text{C} + \gamma \rightarrow \text{C}^+ + \text{e}^-$	Verner et al. (1996)
58	$\text{Si} + \gamma \rightarrow \text{Si}^+ + \text{e}^-$	Verner et al. (1996)

Table 1—Continued

Number	Reaction	Reference
60	$\text{H} + \text{H}(+\text{grain}) \rightarrow \text{H}_2$	Hollenbach & McKee (1979)
61	$\text{H}^+ + \text{e}^-(+\text{grain}) \rightarrow \text{H}$	Weingartner & Draine (2001)
64	$\text{C}^+ + \text{e}^-(+\text{grain}) \rightarrow \text{C}$	Weingartner & Draine (2001)
66	$\text{Si}^+ + \text{e}^-(+\text{grain}) \rightarrow \text{Si}$	Weingartner & Draine (2001)

Note. — The reaction numbering scheme used here is the same as that in paper I. References are to the primary source of data for each reaction.

Table 2. List of Photochemical Reaction Rates.

Number	Reaction	Rate ($J_{21}^{-1} \text{ s}^{-1}$)
51	$\text{H}^- + \gamma \rightarrow \text{H} + \text{e}^-$	$R_{51} = 1.36 \times 10^{-11}$
52	$\text{H}_2^+ + \gamma \rightarrow \text{H} + \text{H}^+$	$R_{52} = 4.11 \times 10^{-12}$
53	$\text{H}_2 + \gamma \rightarrow \text{H} + \text{H}$	$R_{53} = 1.30 \times 10^{-12}$
56	$\text{C} + \gamma \rightarrow \text{C}^+ + \text{e}^-$	$R_{56} = 5.56 \times 10^{-12}$
58	$\text{Si} + \gamma \rightarrow \text{Si}^+ + \text{e}^-$	$R_{58} = 2.44 \times 10^{-11}$

Note. — The reaction numbering scheme used here is the same as that in Paper I. Rates are calculated assuming an incident spectrum corresponding to a modified, diluted 10^5 K black body, as described in the text. The value J_{21} quantifies the strength of the radiation field at the Lyman limit: $J(\nu_\alpha) = 10^{-21} J_{21} \text{ erg s}^{-1} \text{ cm}^{-2} \text{ Hz}^{-1} \text{ sr}^{-1}$. The rate listed for H_2 photodissociation (reaction 53) is for unshielded gas; our treatment of H_2 self-shielding is described in section 2.2.

Table 3. Processes Included in Our Thermal Model.

Process	References
Cooling	
Fine-structure lines (C, C ⁺ , O, Si, Si ⁺)	See Paper I
Ly α cooling	Cen (1992)
H collisional ionization	Janev et al. (1987)
Compton cooling	Cen (1992)
H ⁺ recombination	Ferland et al. (1992)
H ₂ rovibrational lines	Le Boulrot et al. (1999)
H ₂ collisional dissociation	Mac Low & Shull (1986); Martin et al. (1998)
Gas-grain energy transfer ^a	Hollenbach & McKee (1989)
Heating	
Photoelectric effect	Bakes & Tielens (1994); Wolfire <i>et al.</i> (1995)
H ₂ photodissociation	Black & Dalgarno (1977)
UV pumping of H ₂	Burton et al. (1990)
H ₂ formation on dust grains	Hollenbach & McKee (1989)

Note. — a: If $T_{\text{gas}} < T_{\text{grain}}$, the net flow of energy is from the grains to the gas, leading to heating instead of cooling.

Table 4. List of the Runs Discussed in this Paper

Run	Mass(M_{\odot})	Redshift	Z/Z_{\odot}	Dust ^a	J_{21} ^b
S30-Z1	4.0×10^4	30	0.0	No	0.0
I30-Z1	4.8×10^5	30	0.0	No	0.0
I30-L1	4.8×10^5	30	10^{-3}	No	0.0
I25-Z1-ROT ^c	7.8×10^5	25	0.0	No	0.0
I25-Z1	7.8×10^5	25	0.0	No	0.0
I25-L1	7.8×10^5	25	10^{-3}	No	0.0
I25-L1D	7.8×10^5	25	10^{-3}	Yes	0.0
I25-M1	7.8×10^5	25	10^{-2}	No	0.0
I25-M1D	7.8×10^5	25	10^{-2}	Yes	0.0
I25-N1	7.8×10^5	25	10^{-1}	No	0.0
I25-S1	7.8×10^5	25	1.0	No	0.0
I25-S1D	7.8×10^5	25	1.0	Yes	0.0
I25-Z2	7.8×10^5	25	0.0	No	10^{-2}
I25-Z3	7.8×10^5	25	0.0	No	10^{-1}
I25-L3	7.8×10^5	25	10^{-3}	No	10^{-1}
I25-M3	7.8×10^5	25	10^{-2}	No	10^{-1}
I25-M3D	7.8×10^5	25	10^{-2}	Yes	10^{-1}
I25-N3	7.8×10^5	25	10^{-1}	No	10^{-1}
I25-S3	7.8×10^5	25	1.0	No	10^{-1}
I20-Z1	1.5×10^6	20	0.0	No	0.0
I20-L1	1.5×10^6	20	10^{-3}	No	0.0
L30-Z1	4.8×10^6	30	0.0	No	0.0
L30-L1	4.8×10^6	30	10^{-3}	No	0.0
L20-Z1	1.2×10^7	20	0.0	No	0.0
L20-L1	1.2×10^7	20	10^{-3}	No	0.0

^aIndicates whether the run includes dust or only gas-phase metals

^bStrength of the UV background

^cThis run included initial rotation, with a spin parameter $\lambda = 0.05$

Table 5. Halo Mass Resolution and Virial Temperature

Halo mass (M_{\odot})	Redshift	Particle number N	$M_{\text{part}}(M_{\odot})$	$M_{\text{res}}(M_{\odot})$	$T_{\text{vir}}(\text{K})$
4.0×10^4	30	132651	0.25	20	310
4.8×10^5	30	117649	2.0	160	1600
7.8×10^5	25	140608	2.5	200	1900
1.5×10^6	20	140608	5.0	400	2400
4.8×10^6	30	493039	5.0	400	7600
1.2×10^7	20	1042189	5.0	400	9500

Table 6. Physical State of the Densest Gas within the Scale Radius r_s at Time t_{end}

Run	Z^{a} (Z_{\odot})	J_{21}^{b}	$t_{\text{end}}^{\text{c}}$ (Myr)	$T_{\text{c,min}}^{\text{d}}$ (K)	$n_{\text{c,max}}^{\text{e}}$ (cm^{-3})	$x_{\text{H}_2,\text{c,max}}^{\text{f}}$	$f_{\text{sink}}^{\text{g}}$
S30-Z1	0.0	0.0	100	1100	0.3	9×10^{-4}	0.0
I30-Z1	0.0	0.0	75	< 200	> 500	5×10^{-3}	0.04
I30-L1	10^{-3}	0.0	100	< 200	> 500	3×10^{-3}	0.19
I25-Z1-ROT	0.0	0.0	100	< 200	> 500	4×10^{-3}	2×10^{-3}
I25-Z1	0.0	0.0	100	< 200	> 500	4×10^{-3}	0.17
I25-L1	10^{-3}	0.0	100	< 200	> 500	2×10^{-3}	0.20
I25-L1D	10^{-3}	0.0	100	< 200	> 500	0.5	0.13
I25-M1	10^{-2}	0.0	100	< 200	> 500	3×10^{-3}	0.15
I25-M1D	10^{-2}	0.0	100	< 200	> 500	0.5	0.08
I25-N1	10^{-1}	0.0	100	< 200	> 500	2×10^{-3}	0.17
I25-S1	1.0	0.0	100	< 200	> 500	1×10^{-3}	0.28
I25-S1D	1.0	0.0	100	< 200	> 500	0.5	0.27
I25-Z2	0.0	10^{-2}	100	< 200	> 500	5×10^{-4}	5×10^{-3}
I25-Z3	0.0	10^{-1}	100	4400	0.7	1.6×10^{-5}	0.0
I25-L3	10^{-3}	10^{-1}	100	5900	0.6	1.5×10^{-5}	0.0
I25-M3	10^{-2}	10^{-1}	100	5600	0.8	1.7×10^{-5}	0.0
I25-M3D	10^{-2}	10^{-1}	100	5900	0.7	1.5×10^{-5}	0.0
I25-N3	10^{-1}	10^{-1}	100	2600	2.5	5×10^{-5}	0.0
I25-S3	1.0	10^{-1}	100	< 200	> 500	5×10^{-4}	0.3
I20-Z1	0.0	0.0	100	160	1600	3×10^{-3}	0.0
I20-L1	10^{-3}	0.0	100	130	2100	3×10^{-3}	0.0
L30-Z1	0.0	0.0	25	< 200	> 500	7×10^{-3}	1×10^{-3}
L30-L1	10^{-3}	0.0	10	< 200	> 500	3×10^{-3}	2×10^{-4}
L20-Z1	0.0	0.0	20	< 200	> 500	7×10^{-3}	6×10^{-4}
L20-L1	10^{-3}	0.0	10	310	330	3×10^{-3}	0.0

^aMetallicity of the gas.

^bStrength of the UV background.

^cTime at the end of the simulation, or $t = 100$ Myr, whichever is smaller

^dMinimum temperature of the gas within the scale radius r_s .

^eMaximum number density of the gas within the scale radius r_s .

^fMaximum fractional H₂ abundance within the scale radius r_s .

^gMass fraction of gas within a sink particle.

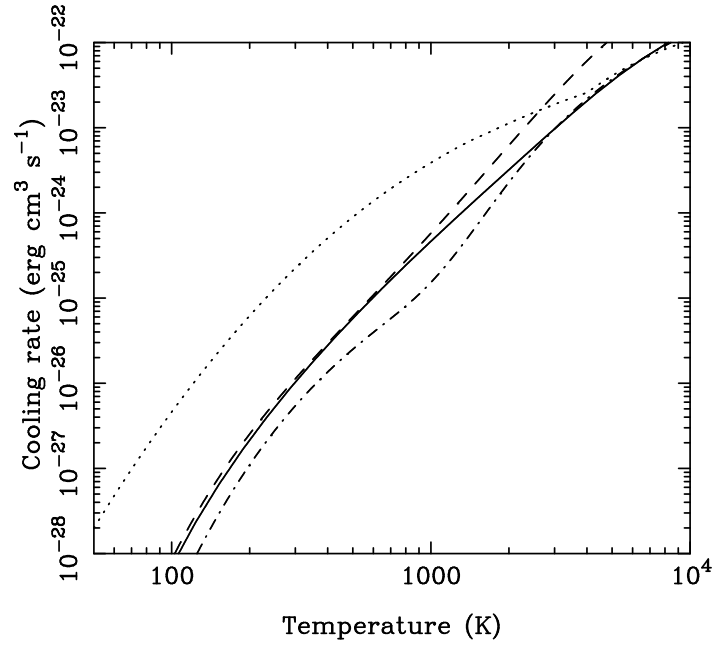


Fig. 1.— Comparison of various parameterizations of the H_2 cooling function, plotted in units of $\text{erg cm}^3 \text{s}^{-1}$. Rates are computed for a number density $n = 1 \text{ cm}^{-3}$ and assuming that $n_{\text{H}} \gg n_{\text{H}_2}$ and that the H_2 ortho-to-para ratio is 3:1. *Solid line*: Le Bourlot et al. (1999); *dashed line*: Galli & Palla (1998); *dotted line*: Lepp & Shull (1983); *dash-dotted line*: Hollenbach & McKee (1979).

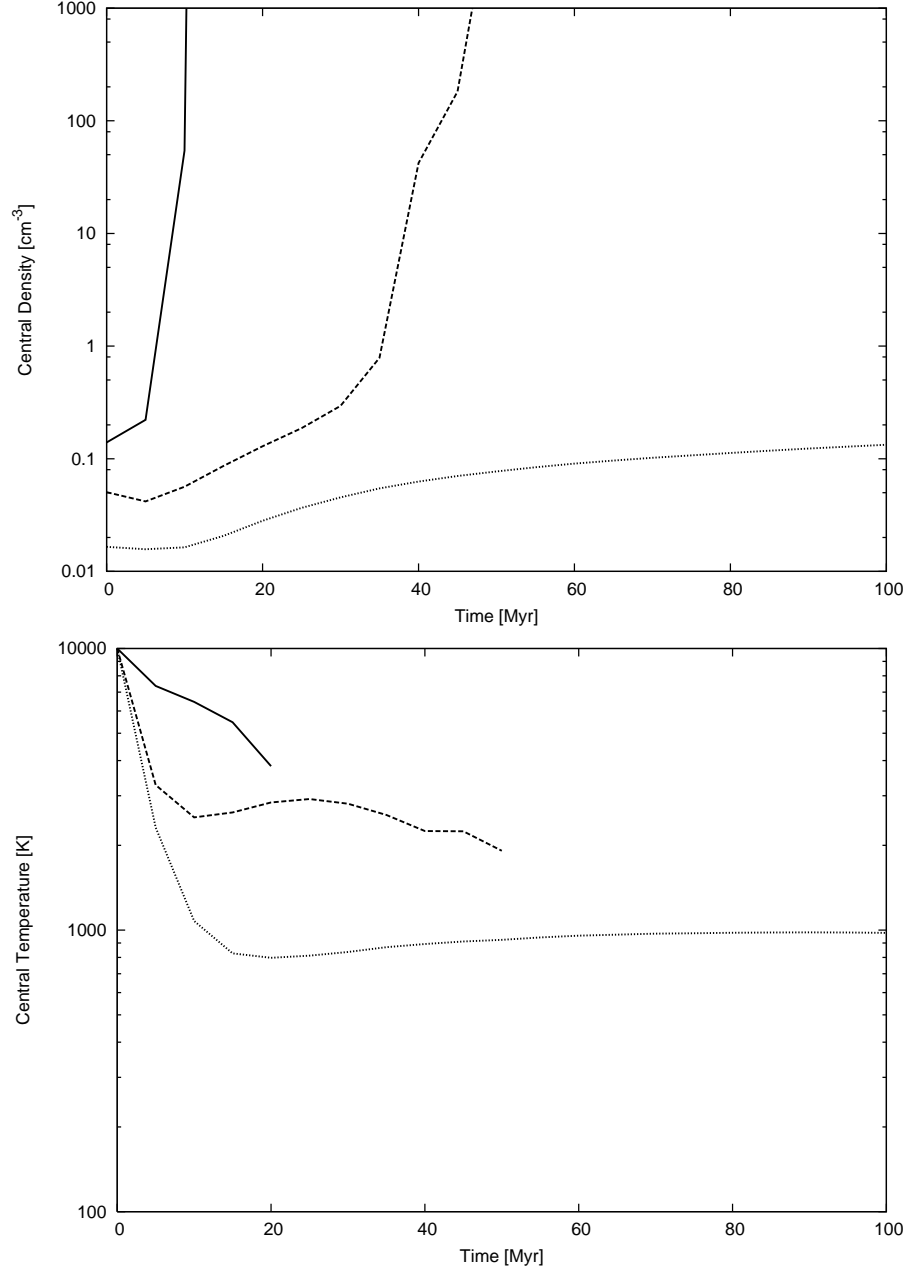


Fig. 2.— Top: Time evolution of the gas density within the scale radius r_s of the dark matter halo in runs L30-Z1 (*solid line*), I30-Z1 (*dashed line*), and S30-Z1 (*dotted line*), corresponding to halos with masses 4.8×10^6 , 4.8×10^5 , and $4.0 \times 10^4 M_\odot$, respectively. Bottom: Same as the top panel, but for the central temperature of the gas.

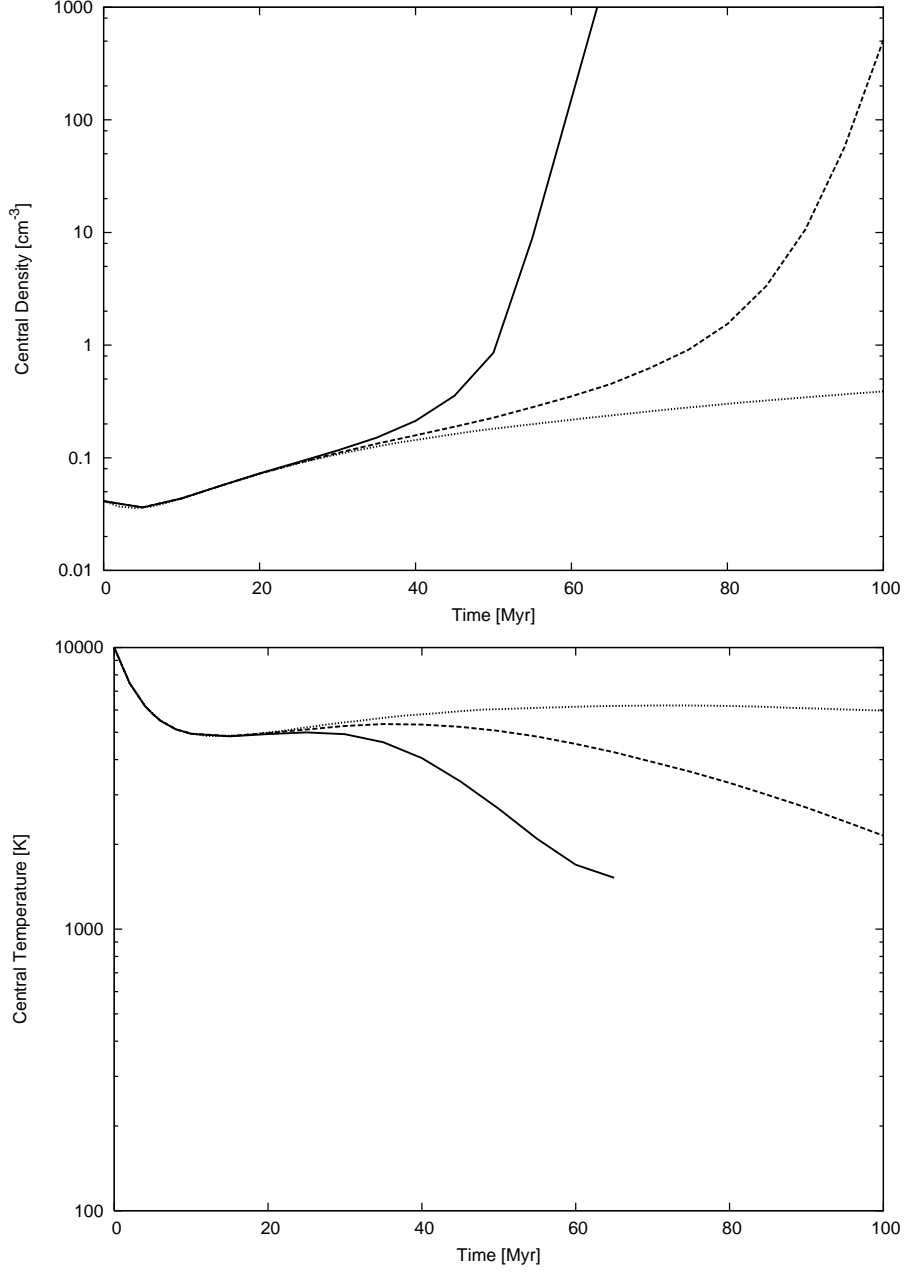


Fig. 3.— Top: Same as the top panel of Fig. 2, but for runs I25-Z1 (*solid line*), I25-Z2 (*dashed line*), and I25-Z3 (*dotted line*). These runs were started at $z = 25$ with a halo mass $M = 7.8 \times 10^5 M_\odot$, and had UV background field strengths $J_{21} = 0.0, 0.01$, and 0.1 , respectively. Bottom: Same as the top panel, but for the central temperature of the gas.

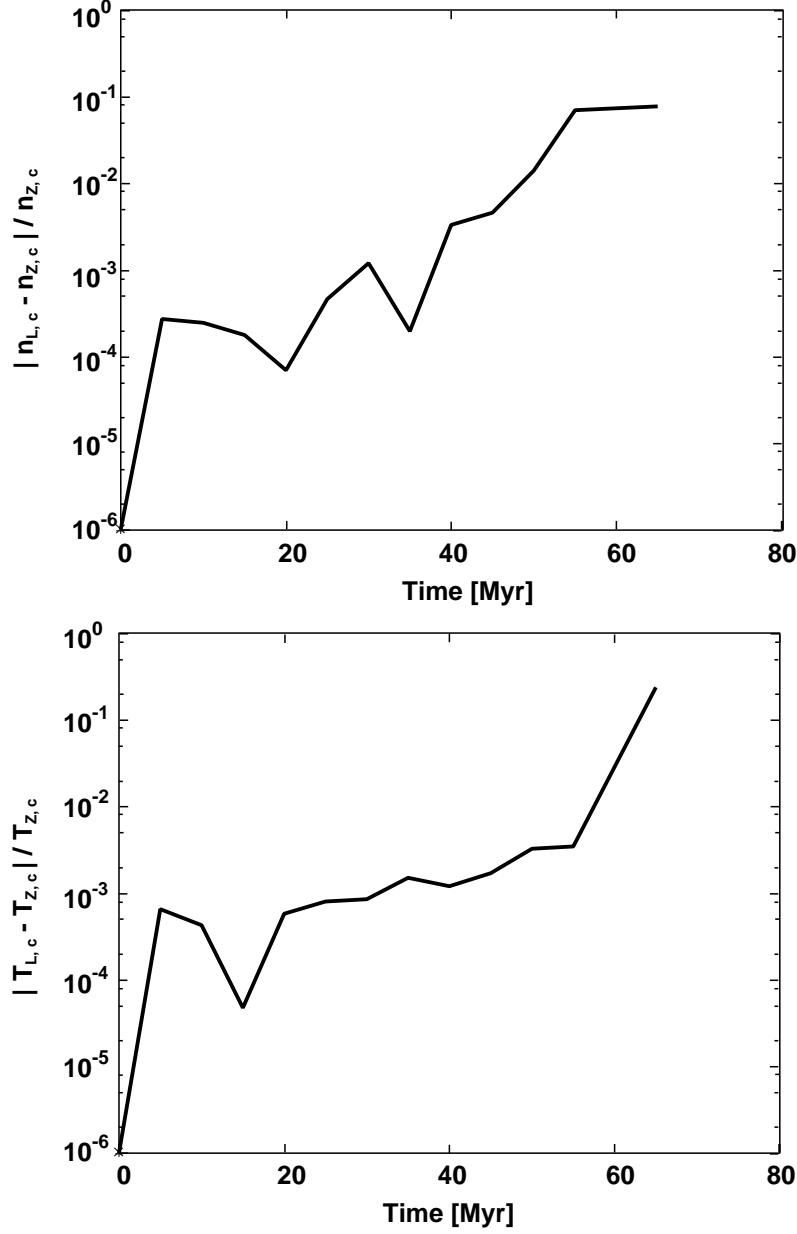


Fig. 4.— Top: Time evolution of the relative difference $|n_{Z,c} - n_{L,c}|/n_{Z,c}$, where $n_{L,c}$ is the central gas density in run I25-L1 and $n_{Z,c}$ the central density in run I25-Z1. For clarity, we only plot the evolution until the point at which a sink particle forms (or until the end of the run, if no sink forms). Bottom: Same as the top panel, but for the relative difference between the central temperature in the two runs.

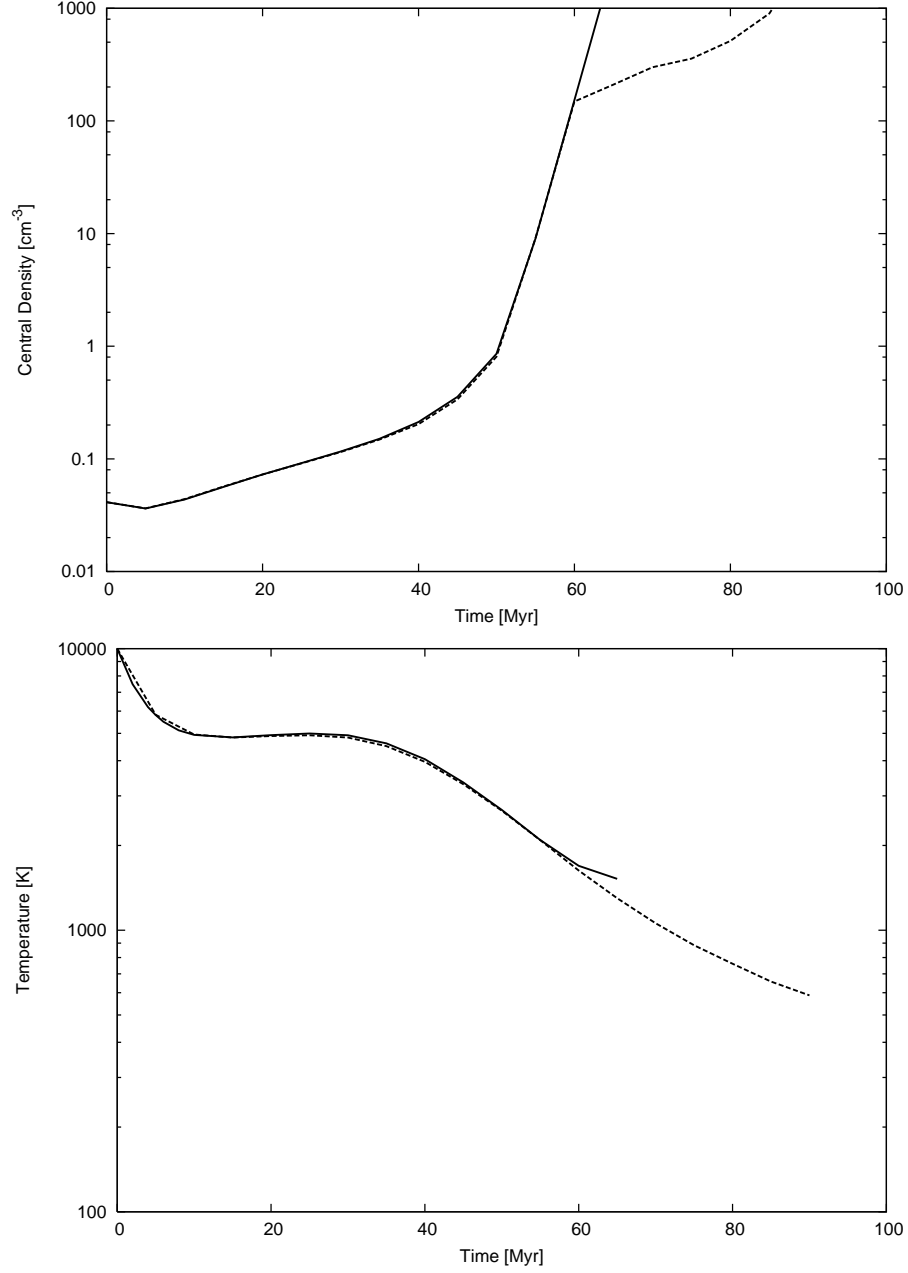


Fig. 5.— Top: Time evolution of the gas density within the scale radius r_s of the dark matter halo in runs I25-Z1 (*solid line*) and I25-Z1-ROT (*dashed line*). Bottom: Same as the top panel, but for the central temperature of the gas

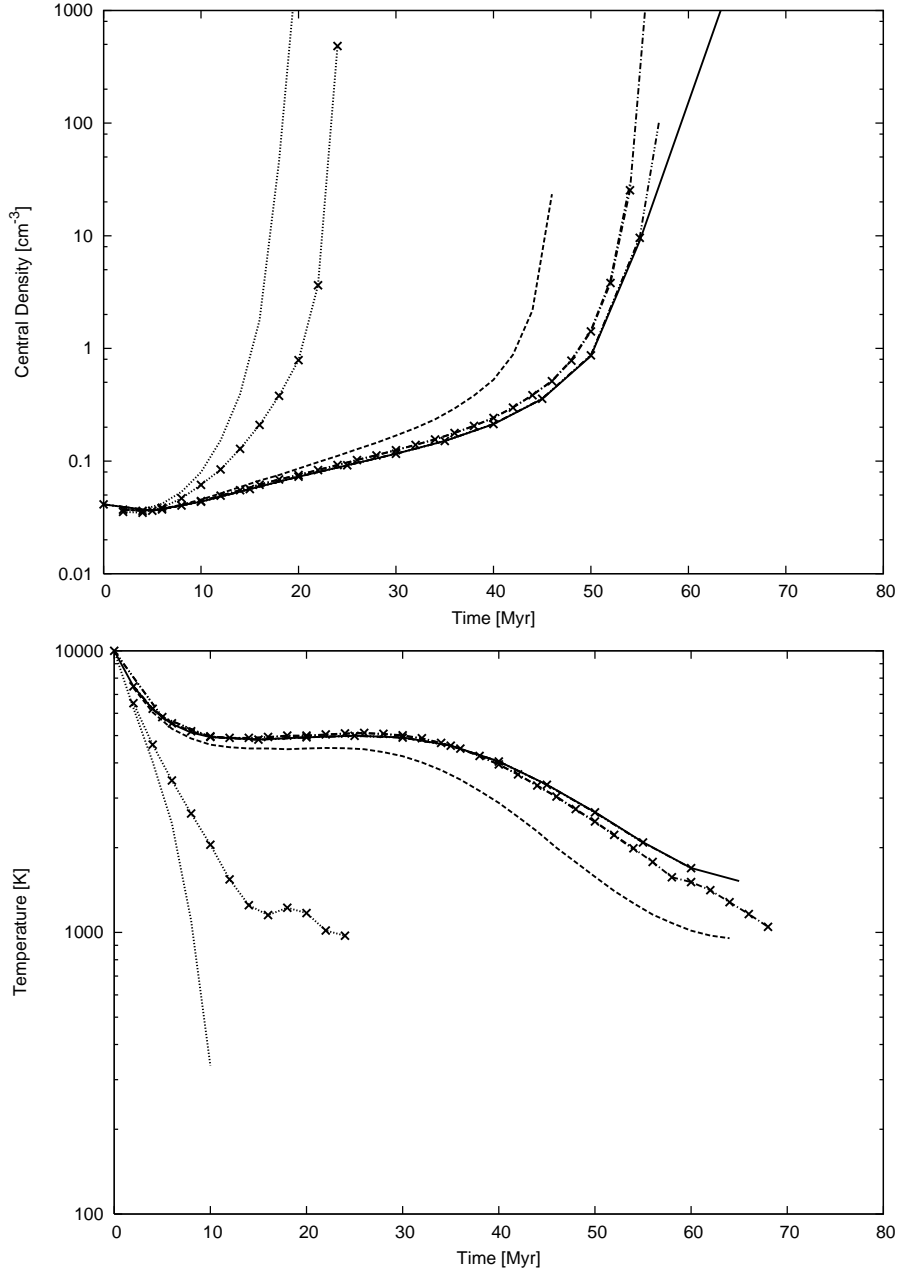


Fig. 6.— Top: Time evolution of the gas density within the scale radius r_s of the dark matter halo in runs I25-Z1 (*solid line*), I25-L1 (*dot-dot-dashed line*), I25-M1 (*dash-dotted line*), I25-N1 (*dashed line*), and I25-S1 (*dotted line*), which have metallicities $Z = 0.0, 10^{-3}, 10^{-2}, 0.1$, and $1.0 Z_\odot$, respectively. We also include three runs with dust, I25-L1D, I25-M1D, and I25-S1D, denoted by the lines with symbols. In all of these runs, the halo mass $M = 7.8 \times 10^5 M_\odot$ and the run begins at a redshift $z = 25$. No ultraviolet background is present in any of these runs. Bottom: Same as the top panel, but for the central temperature of the gas.

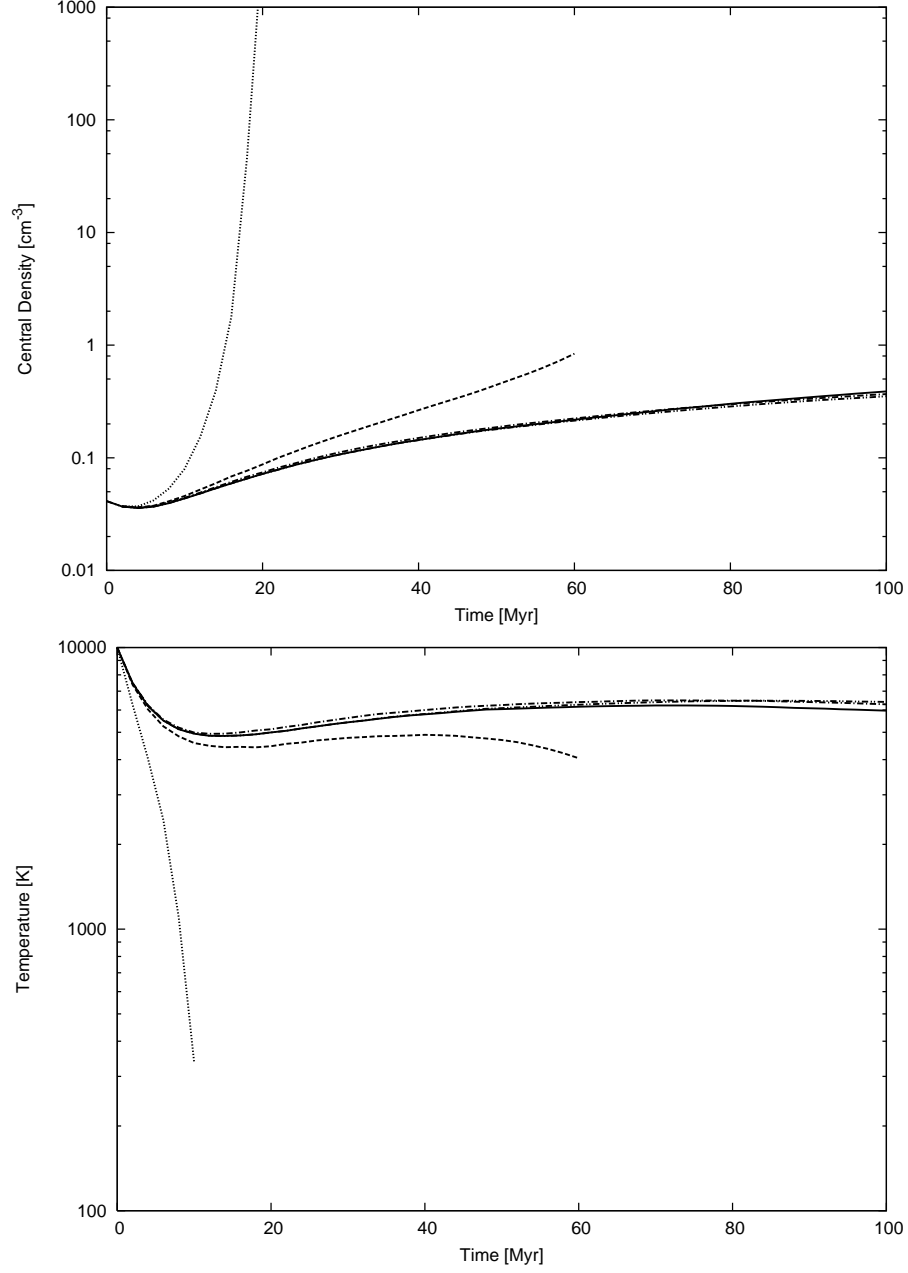


Fig. 7.— Top: Same as Fig. 6, but for runs I25-Z3 (*solid line*), I25-L3 (*dot-dot-dashed line*), I25-M3 (*dash-dotted line*), I25-N3 (*dashed line*), and I25-S3 (*dotted line*). The UV background field strength in all of these runs was $J_{21} = 0.1$. Bottom: Same as the top panel, but for the central temperature of the gas.

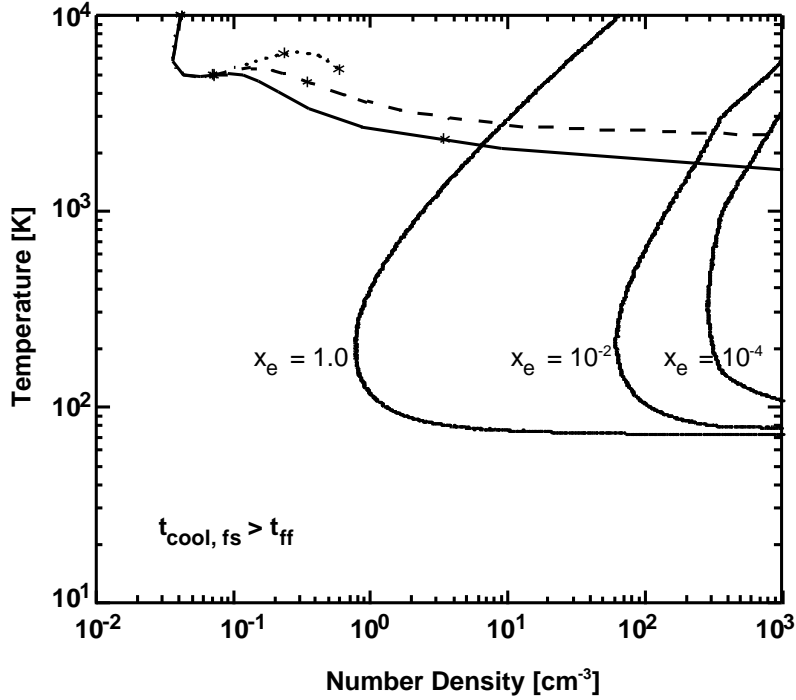


Fig. 8.— *Solid contours*: Temperature and density at which the cooling time due to fine-structure emission, $t_{\text{cool,fs}}$, equals the free-fall time, t_{ff} , for gas with a metallicity $Z = 10^{-3} Z_{\odot}$ and with fractional ionizations $x_e = 1.0$, 10^{-2} , and 10^{-4} . To the left of each line, $t_{\text{cool,fs}} > t_{\text{ff}}$, so metal cooling is inefficient. In every case, we assume that all of the carbon and silicon is present as C^+ and Si^+ , respectively. In the $x_e = 1.0$ case, we assume that all of the oxygen is present in the form of O^+ , but otherwise that it is all O. To compute the free-fall time, we take the density to be the sum of the gas density ρ_g and the dark matter density at the center of the halo ρ_{dm} . The figure also shows how the temperature and density of the gas at the centre of the halo evolve in runs I25-L1 (*solid line*), I25-L2 (*dashed line*), and I25-L3 (*dotted line*). The evolution of the fractional ionization in these runs is indicated by the star symbols: $x_e = 1.0$ for $T = 10^4$ K, and decreases by a factor of 10 between each successive star.